High Performance PEEK/Carbon Nanotube Composites Compatibilized with Polysulfones-I. Structure and Thermal Properties.

Ana M. Díez-Pascual[a,*], Mohammed Naffakh[a], José M. González-Domínguez[b], Alejandro Ansón[b], Yadienka Martínez-Rubi[c], M. Teresa Martínez[b], Benoit Simard[c], Marián A. Gómez[a]

[a]Departamento de Física e Ingeniería de Polímeros. Instituto de Ciencia y Tecnología de Polímeros, CSIC, c/ Juan de la Cierva 3, 28006 Madrid, Spain.

[b]Departamento de Nanotecnología. Instituto de Carboquímica, CSIC, c/ Miguel Luesma Castan 4, 50018 Zaragoza, Spain.

[c]Steacie Institute for Molecular Sciences, NRC, 100 Sussex Drive, Ottawa, Canada.

ABSTRACT

Poly(ether ether ketone) (PEEK)/single-walled carbon nanotube (SWCNT) composites incorporating polysulfones as compatibilizers were fabricated by melt-blending, after pre-processing based on ball milling and mechanical treatments in an organic solvent. Their structure, morphology and thermal properties have been investigated. Microscopic observations showed a uniform distribution of the CNTs and good miscibility between the compatibilizer and matrix phases. The incorporation of wrapped SWCNTs leads to a remarkable increase in the degradation temperatures of the matrix in comparison with non-compatibilized samples, attributed to the high thermal stability of the polysulfones and the compatibilizing effect. The addition of very small CNT loadings raises the crystallization temperature and the degree of crystallinity of PEEK. At higher concentrations, the inactive nucleating activity of the nanofillers, the confinement of the polymer chains within the CNT network and the presence of an amorphous compatibilizer moderately hinder PEEK

[*]Corresponding author. Fax: +34 915 644 853.
E-mail address: adiez@ictp.csic.es (A. M. Díez-Pascual)

crystallization. Synchrotron X-ray diffraction experiments indicate the existence of reorganization phenomena of the matrix crystals during the heating of the composites. Improved thermal properties are found for composites incorporating arc-purified SWCNTs, attributed to the higher degree of debundling and lower metal content of these CNTs. These compatibilized composites are new materials for potential high-temperature structural applications.

1. Introduction

Carbon nanotube (CNT) reinforced composites have attracted a great deal of interest for many applications due to their outstanding mechanical, electrical and thermal properties [1,2] arising from the nanoscale dimensions, excellent physics characteristics and exceptionally high aspect ratio of nanotubes [3,4]. Achieve a good dispersion of the reinforcement in the polymer matrix is the key to fabricate composites with enhanced properties; however, this is commonly a difficult task due to the strong tendency of the nanotubes to gather and form bundles. To improve their distribution through the matrix, different processing routes such as solution mixing [5] and *in situ* polymerization [6] have been employed. Moreover, other strategies have been used depending on the nature of the interactions between CNTs and polymers (i.e. covalent linkage, assembly and compounding previously functionalized CNTs with the polymer, dispersion of CNTs in compatibilizing agents [7]).

Poly(aryl ether ketone)s (PAEKs) such as PEEK are an important class of high performance engineering thermoplastics displaying a unique combination of thermal stability, chemical and solvent resistance, excellent mechanical properties over a wide temperature range and good fire resistance [8,9]. These polymers can be processed by conventional techniques, such as extrusion and compression molding, and can be applied as matrix resins for reinforced composites. Compared to poly(arylene ether sulfone)s, which are usually amorphous polymers and subject to attack by solvents, PAEKs are semicrystalline and

therefore resistant to solvents, which is a critical factor in an aerospace environment. However, due to their insolubility and high melting points (generally above 300 ºC), these polymers need to be processed under specific conditions. Since its commercialization, PEEK has been used in a wide range of applications, from medicine to the electronics, telecommunication and transport industries (automobile, aeronautic and aerospace) [10]. Over the last decades many studies have been reported on the structural [11], mechanical [12] and thermal [13] characterization of this linear aromatic polymer, albeit only a few papers deal with such composites made of a PEEK matrix; the most relevant are those published by Shaffer *et al.* [14], working with vapor-grown carbon nanofiber/PEEK composites, Deng *et al.* [15], dealing with multi-walled carbon nanotube (MWCNT)/PEEK nanocomposites, and Song *et al.* [16], who prepared sandwich like SWCNT paper/PEEK composites. Recently, our group reported the synthesis and characterization of PEEK/SWCNT composites [17]. We have developed strategies to efficiently incorporate the nanotubes in the PEEK matrix. An excellent approach would be to previously wrap the SWCNTs in this polymer. However, its insolubility in common organic solvents makes difficult to perform a wrapping process in liquid media.

Polysulfones (PSFs) are high performance amorphous thermoplastics well known for their toughness and stability at high temperatures [18]. Transparent, rigid and high-strength polymers, they exhibit excellent impact resistance over a wide temperature range and are highly resistant to water, steam, acids and oxidizing agents [19]. Their structure is formed by a monomeric unit which contains phenyl, ether and sulfone moieties. The phenyl rings give thermal stability to the polymer, enhanced by the high degree of resonant stabilization. Sulfone groups are very electron-withdrawing, and their proximity to benzene rings provides high thermal and oxidative resistances. The ether groups confer some flexibility, which leads to an inherent toughness [20]. These thermoplastics, widely used for medical and household

appliances, are also employed in the electronics and automotive industries. In this work, they were chosen as compatibilizers due to their similar structure to the polymer matrix, miscibility with it at very low PSF content [21], chemical compatibility with both components of the composite and solubility in common organic solvents. The sp^2 hexagonal networks of the SWCNTs are expected to undergo Л interactions with the aromatic moieties of the polysulfones. Furthermore, the oxygen groups (mainly carboxylic, but also others as phenol or aldehyde) generated onto the surface and tips of acid-treated SWCNTs are capable of forming hydrogen bonds with the highly polar segments of the PSFs chains. Likewise, the phenyl and bisphenol-A moieties of the compatibilizers would interact with the polymer matrix through Л-Л stacking. Therefore, the dual affinity of the polysulfones with the filler and matrix is expected to rule the wrapping process and the compatibilization effect. In the literature, several papers have been focused on the morphological [21], thermal [18] and mechanical characterization [22] of PEEK/PSF mixtures. However, to best of our knowledge, there is no previous attempt to employ polysulfones as compatibilizers for polymer/CNT composites.

The present article deals with the study of PEEK/SWCNT reinforced composites incorporating two different polysulfones as compatibilizing agents. To investigate their efficiency, different types of wrapped SWCNTs, at various filler loadings, have been incorporated in the polymer matrix following a processing route based on ball milling and mechanical pre-treatments in ethanol media. An extensive characterization has been carried out to analyze in detail the influence of the compatibilizers as well as SWCNT type and concentration on the morphology, structure and thermal properties of these new composites for high-temperature structural applications.

2. Experimental

2.1. Materials

PEEK 150P used in this study was provided in coarse powder form by Victrex plc, UK. This low viscosity grade, the most suitable for potential aircraft structural applications, presents the following physical characteristics: $M_w \sim 40000$ g/mol, $T_g = 147$ ºC, $T_m = 345$ ºC, $d_{25ºC} = 1.32$ g/cm^3, $\eta_{350ºC} \sim 10^3$ Pa·s; its chemical structure is shown in Fig. 1. The arc discharge SWCNTs were synthesized at the Institute of Carbon Chemistry (ICB-CSIC), Zaragoza, Spain, using graphite electrodes and Ni/Y~4/1 atomic % as catalyst [23]. These SWCNTs were purified following an experimental procedure inspired in the method developed by Yu *et al.* [24]. They were refluxed in HNO_3 7M at 150°C for 4 h. The resulting mixture was bath sonicated for 30 min, and centrifuged at 3500 rpm for 15 min. The supernatant was decanted off, and the sediments were redispersed in H_2O/HCl at pH~2. Centrifugation was repeated twice to maximize the removal of amorphous carbon impurities [25]. The final sediment was redispersed in deionized water, sonicated for 3 h, and centrifuged at 13000 rpm several times. The resulting SWCNT dispersions were observed to be stable for several weeks; they were filtered through 1.2 μm pore size polycarbonate membranes, dried in an oven at 80-100 °C, and milled in an agate mortar. The carboxylic groups counteract the van der Waals attractive forces between CNTs and increase their polar character, which enhances the anchoring of compatibilizers and their integration into the polymer matrix. Laser-grown SWCNTs were prepared at the Steacie Institute for Molecular Sciences (SIMS-NRC), Canada, using an approach to the two-laser synthesis method [26]. The as-received samples were used without further purification.

The compatibilizing agents (Fig. 1), poly(bisphenol-A-ether sulfone), PSF ($M_w \sim 35000$ g/mol, $T_g = 201$ ºC, $d_{25ºC} = 1.24$ g/cm^3), and poly(1-4-phenylene ether-ether sulfone), PEES ($M_w \sim 38000$ g/mol, $T_g = 192$ ºC, $d_{25ºC} = 1.37$ g/cm^3), were provided by Sigma-Aldrich in pellet form. The SWCNTs were wrapped by these polymers in liquid media: 25 mL of a PSF 1,4-dioxane or PEES 1-methyl-2-pyrrolidone (NMP) solution (both at 1.5% w/w) were mixed

with ~260 mg of SWCNTs (either laser as-grown or acid treated arc-discharge) with bath sonication for 5 min. Each mixture was treated with a Hielscher DRH-UP400S ultrasonic tip (400 W maximum power; 24 kHz maximum frequency) for 60 min at 50% oscillation amplitude and 50% cycle time. The resulting dispersion was observed to be highly stable. Then it was filtered using a 0.1 μm pore size PTFE membrane and finally dried under vacuum at 60 ºC during 2 or 24 hours (for 1,4-dioxane or NMP respectively) to assure total evaporation of the solvent. In order to homogenize the particle size, the resulting solid was milled in an agate mortar.

A complete characterization of the solid SWCNT dispersions in the compatibilizing agents was carried out by SEM, TEM, X-ray diffraction, FT-Raman spectroscopy and TGA; these results will be discussed in a following section.

2.2. Preparation of PEEK/SWCNT composites

The composites were prepared following a procedure based on the use of mechanical treatments in organic solvent. Before blending, the polymer was vacuum dried at 120 ºC for 4 h to minimize the effects of moisture and ground with a ball mill in order to reduce its particle size. After, the fine polymer powder was manually mixed with the SWCNTs wrapped in the compatibilizing agents (see nomenclature in Table 1). Each mixture PEEK/SWCNT was dispersed in a small volume of ethanol and then homogenized by mechanical stirring and bath ultrasonication for approximately 30 min (a compromise between achieving sufficient dispersion and minimizing CNT damage). Subsequently, the dispersion was partially dried in vacuo at 50 ºC under a pressure of about 70 mbar for 5 min; the bath sonication and drying steps were repeated successively until the solvent was completely removed.

The melt-compounding was performed in a Haake Rheocord 90 extruder operating at 380 ºC, with a rotor speed of 150 rpm, using mixing times of 20 min. For comparative purposes, samples including non-wrapped SWCNTs, as well as reference PEEK/PSF and

PEEK/PEES blends containing the same amount of compatibilizer as the PEEK/SWCNT (1 wt%) composites were also prepared in the same way. The samples were allowed to cool to ambient temperature and then divided into smaller pieces. These were pressed into thin films (0.5 mm thick) at 380 ºC under 130 bar and refrigerated between metal plates at 15 ºC, to be employed for the different measurements.

2.3. Scanning and transmission electron microscopies

The morphology of the SWCNTs and the composites was examined with a Philips XL 30 scanning electron microscope (SEM) using an acceleration voltage of 25 kV and an intensity of $9 \cdot 10^{-9}$ A. The composite samples were cryo-fractured from film specimens and then coated with a 5 nm overlayer of an Au-Pd (80-20) alloy in a Balzers SDC 004 evaporator, using a covering time of 242 s at 20 mA, to avoid charging during electron irradiation.

Transmission electron microscopy (TEM) images of the SWCNTs wrapped in polysulfones were obtained with a Philips Tecnai 20 FEG (LaB_6 filament) analytical electron microscope fitted with an EDAX thin-window energy dispersive X-ray detector, operating at 200 kV and with 0.3 nm point-to-point resolution. Samples were prepared by re-suspending in an ultrasonic bath about 2 mg of wrapped SWCNTs in 5 mL of 1,4-dioxane or NMP (for PSF or PEES respectively). A drop of each suspension was cast on 200 mesh Carbon Lacey copper grids and dried with a small flow of air. At least 20 TEM micrographs of each type of SWCNT wrapped in both compatibilizers were examined to assess the homogeneity of the dispersions.

2.4. FT-Raman spectroscopy

The FT-Raman Spectra of the SWCNTs were performed using a HORIBA Jobin Yvon Raman spectrometer model HR 800 UV, working with a 532 nm laser excitation source; the data were analysed with NGS LabSpec software. At least 3 different spectra were recorded for each nanotube sample, and those reported are the corresponding averages.

2.5. Thermogravimetric analysis

Thermogravimetric analysis (TGA) of the SWCNTs and the composites was conducted using a TA-Q500 thermobalance; prior to the measurements, treated SWCNTs were dried overnight at 100 ºC to assure total evaporation of the solvent. Samples of ~5 mg were ramped at a heating rate of 10 ºC/min, from room temperature to 900 ºC, with a gas purge of 150 mL/min. The analysis was performed under both nitrogen and dry air atmospheres.

2.6. Differential scanning calorimetry

Dynamic DSC experiments were carried out in a Mettler TA4000 differential scanning calorimeter, equipped with a DSC-30 oven with automatic temperature control, operating under nitrogen flow. Samples with an average mass of 12 mg were melted at 380 ºC and maintained at this temperature for 5 min to erase the thermal history of the material. Subsequently, several cooling and heating cycles were performed at rates of 2, 5, 10 and 15 ºC/min, in the temperature range between 30 and 380 ºC.

The transition temperatures were taken as the peak maximum or minimum in the calorimetric curves. The degree of crystallinity of PEEK composites was calculated from the normalized peak enthalpies according to the relation: $X_m = \Delta H_{m,PEEK} / (\Delta H°_{m,PEEK} \times w_{PEEK})$ where $\Delta H_{m,PEEK}$ is the apparent melting enthalpy of PEEK, w_{PEEK} is the weight fraction of PEEK in the composites and $\Delta H°_{m,PEEK}$ is 130 J/g, the theoretical value of enthalpy for a 100% crystalline PEEK sample [27].

2.7. X-ray diffraction

Simultaneous small and wide-angle X-ray scattering (SAXS/WAXS) experiments using synchrotron radiation were performed at the A2 beamline of the HASYLAB synchrotron (DESY, Hamburg). The beam was monocromatized by Bragg reflection through a germanium single crystal ($\lambda = 0.15$ nm). Linear Gabriel detectors were used to collect the scattered light. The sample to detector distance for SAXS was 236 cm, and for WAXS 135 mm, being wide angle diffractograms registered in the range of $2\theta = 10 - 34º$. The scattering angle of the

SAXS and WAXS patterns were calibrated with a RTT (rat tail tendon) and a PET standard, respectively. To ensure adequate temperature control, samples covered by aluminium paper were thermostated inside a vacuum system. The methodology used in the crystallization and melting experiments of the nanocomposites was similar to that described for the calorimetric measurements. Diffractograms were recorded with an acquisition time of 30 s, employing a total cycle time of 35 min. The degree of crystallinity X_c of the composites was calculated using the following relation: $X_c = I_c / (I_c + I_a)$, being I_c and I_a the integrated intensities of the crystalline and amorphous phases, respectively.

Room temperature X-ray diffraction data of the SWCNT dispersions were collected with a Bruker D8 Advance diffractometer using a Cu tube as X-ray source (λ CuKα = 1.54 Å), with a voltage of 40 kV and an intensity of 40 mA. The results were analyzed with the fitting software Topas 2.1 in Bragg-Brentano geometry in the angular range of $2\theta = 3^\circ - 80^\circ$, with angular increment of 0.05º and accumulation time of 3 s.

3. Results and discussion

3.1. Characterization of the SWCNT dispersions

The SWCNTs wrapped in the polysulfones were extensively characterized by different techniques before proceeding to the preparation of the composites; these results are summarized in Table 1.

SEM analysis of the SWCNT dispersions revealed a non-homogeneous size distribution of the diameters. On average, arc-purified SWCNTs dispersed in the polysulfones present smaller bundle diameter (D) than the corresponding laser-grown SWCNTs. Moreover, SWCNTs dispersed in PEES exhibit slightly lower D than those wrapped in PSF; nevertheless, considering the broad distribution of the diameters and the detection limit of the technique (about 10 nm), the values of D obtained should be considered only an approximation.

Typical TEM micrographs of arc-purified and laser-grown SWCNTs wrapped in PEES are displayed in Fig. 2. Good homogeneity in the dispersions, without agglomerates, was observed from the images; this confirms the efficiency of the wrapping process in liquid media. It is important to notice that the effective debundling attained in the wrapped SWCNTs is caused by the presence of the polysulfones, which impedes the re-aggregation of the nanotubes after the evaporation of the solvent. Small CNT bundles (2-4 individual tubes), which appear as fine stripes, are clearly shrouded in the amorphous polymer, suggesting that the SWCNT frameworks remained structurally intact after the wrapping. No voids or discontinuities are found between the nanotube and polymer phases; the polysulfone wraps around the bundles forming a tight interfacial layer. It is worth noting that improved dispersion and interfacial adhesion CNT-polysulfones are prerequisites to fabricate composites with enhanced thermal and mechanical properties. In general, wrapped laser-grown SWCNTs present thicker bundles than arc-purified CNTs, in agreement with SEM analysis (Table 1).

X-ray diffraction patterns of the different SWCNTs are shown in Fig. 3. Intense bundle lattice peaks, appearing at low diffraction angles [28] (see the arrows marked on the plot), can be visualized in the diffractogram of pristine laser-grown SWCNTs (Fig. 3a). The synthesis procedure of these nanotubes provides a material with thick rope-like bundles of CNTs which are present since they were used without further purification. The wrapping process in the polysulfones induced nanotube disaggregation, as revealed by the noticeable diminution or disappearance of the bundle peaks. Notice that the main feature bands of the pure polysulfones are low intense and appear in the angular range $2\theta = 17 - 25^{\circ}$; therefore, they practically do not interfere with the bundle lattice peaks, as seen in Fig. 3c. In the arc-purified SWCNTs (Fig. 3b), the absence of metal catalysts diffractions (Ni peaks at $2\theta = 44.4$ and 51.9°) evidences the successful removal of metallic impurities during the purification treatment. Moreover, most of the bundle peaks of the non-wrapped arc-purified SWCNTs could hardly be detected (only a

slightly visible maximum at $2\theta \approx 6^{o}$), which might point to a pre-debundling induced by the purification process. The indicated lattice peak is even less intense for the arc-purified SWCNTs wrapped in PSF, and practically disappears when the nanotubes are dispersed in PEES. The polysulfone bands seem to contribute slightly to the diffraction pattern of the arc-purified wrapped SWCNTs (Fig. 3b), being this influence stronger for those shrouded in PEES, as revealed by the higher intensity ratio of its bands in comparison with the graphite peak ($2\theta = 26.6$). This is perfectly consistent with the polysulfone content measured by TGA (see Table 1). Overall, the comparison of the different diffractograms indicates that the acid-treated SWCNTs wrapped in the polysulfones are the most effectively debundled.

The FT-Raman spectra of the SWCNTs and their dispersions in both polysulfones (Fig. 4) were recorded to analyze possible changes in the bands due to the CNT disaggregation. All the samples display almost identical spectra, with four main features [29]: the tangential modes or G-band at ~1600 cm^{-1}, the dispersive disorder induced D-band around 1350 cm^{-1}, its second order related harmonic G´-band near 2650 cm^{-1}, and the radial breathing mode (RBM) at ~200 cm^{-1}. The Raman spectra of arc-purified (Fig. 4a) and laser-grown (Fig. 4b) SWCNTs showed that the dispersion of the CNTs in both polysulfones produced modifications in the G/D intensity ratios, indicating changes in their vibrational modes. Moreover, the comparison of the spectra for CNTs synthesized by different methods reveals a lower G/D ratio for arc-purified SWCNTs, likely arising from a more intense D-band. Taking into account that the relative strength and width of the D-band can be used as a qualitative measurement of the fraction of CNTs with imperfections present in the sample, this observation suggests higher defect content in this type of SWCNTs, probably originated during the purification treatment in nitric acid.

The Raman shift of the RBM is inversely proportional to the SWCNT diameter, and reflects the tube diameter distribution in the SWCNTs excited with this particular wavelength. The position of the RBM has been reported to be strongly influenced by the nanotube packing,

doping and wrapping [30]. In the case of arc-purified SWCNTs, no appreciable change is found in the RBM part of the spectra after the dispersion process in the compatibilizers. In contrast, for laser-grown SWCNTs (Fig. 4c), a pronounced upshift of ~12 cm^{-1} is observed in the maximum RBM peak from the pristine nanotubes to the polysulfone-wrapped material. This is a clear proof of the debundling caused by the polysulfones, as this RBM displacement has been previously attributed to a polymer intercalation among individual SWCNTs in a bundle [31]. These observations are in good agreement with those derived from the X-ray diffractograms.

TGA under air atmosphere was carried out to obtain information about the thermo-oxidative stability of the CNT samples and determine their metallic residue. The temperatures of maximum rate of weight loss (T_{mr}) for the wrapped SWCNTs are collected in Table 1. Higher oxidation temperatures are associated with purer and less defective materials [32]. Although highly purified and defect-free SWCNTs will oxidize at temperatures ≥ 700 ºC, it has been shown that the presence of even small quantities of impurity carbons can induce oxidation at lower temperatures [33]. Moreover, the position of T_{mr} peak is also strongly affected by the amount and morphology of the metal impurities. The residual mass corresponds to the oxidized catalyst particles, and provides an upper limit to the abundance of metal in the samples. As expected, purified arc-grown SWCNTs, with a lower content of metal impurities, present improved thermal stability than as-grown laser-SWCNTs. With regard to the amount of compatibilizer retained by the SWCNTs, it can be seen from Table 1 that the dispersions retain more PEES than PSF, attributed to the higher polarity of the former polysulfone, and the AP-PEES sample exhibits the highest compatibilizer content.

3.2. Carbon nanotube dispersion in the composites

The homogeneous dispersion of the SWCNTs in the polymer matrix is one of the most important features for reinforcing the composites, since any heterogeneity or aggregation

could result in structural defects, which would have detrimental effects on the mechanical properties. The state of dispersion and morphology of PEEK composites was qualitatively visualized by SEM. Fig. 5 shows typical micrographs at different magnifications of compatibilized films containing 1.0 wt% laser-grown SWCNTs; similar images were obtained from samples prepared with arc-purified SWCNTs. For all the samples analyzed, only two phases were observed, indicating good miscibility between the compatilibizer and PEEK. The CNTs (which appear as bright spots) are found to be randomly and well-dispersed within the matrix by the combination of ultrasonication and shear force from melt-blending (see arrows marked on the image). No CNT agglomerations or entanglements were observed in the whole examined areas; the energy of the sonication process breaks up the aggregates, leading to a fine dispersion of the SWCNTs, which results in a large CNT-matrix effective contact area. Moreover, no open ring holes or voids were observed around the SWCNTs, hinting at the existence of good filler-matrix interfacial adhesion. It is worthy to notice that the average bundle diameters of the SWCNTs dispersed in PSF and PEES (Table 1) are smaller than the values obtained from SEM images of the non-wrapped SWCNTs [17]. This indicates that the addition of the polysulfones leads to a significant CNT disentanglement and debundling, and thereby confirms their efficiency as compatibilizing agents. The satisfactory dispersion of the SWCNTs in the composites is attributed to the effective pre-mixing stage under ultrasonic vibration in ethanol as well as to the use of compatibilizers miscible and structurally similar to the PEEK matrix.

3.3. Thermal stability

To analyze the influence of the CNTs and the compatibilizers on the thermal stability of these composites, TGA was carried out under both oxidative and inert atmospheres. The degradation curves of PEEK composites containing different amounts of laser-grown SWCNTs dispersed in PSF are displayed in Fig. 6. Similar behavior was found for the other samples tested. It is

clear that the stability of the composites depends strongly on the type of atmosphere: under inert conditions all the samples exhibit a rapid single decomposition stage, with a residual weight at 650 ºC ranging between 55-60%, due to the remaining ether and aromatic structures [34] as well as the SWCNTs; therefore, this residual mass rises slightly with increasing CNT content. In contrast, under oxidative atmosphere two consecutive steps are observed, the second considerably smoother, and the major weight loss (~65%) occurs during this latter stage, which leads to the total decomposition of the materials. Under both conditions, the integration of increasing CNT loadings leads to a progressive rise in the matrix degradation temperatures: the largest improvements are found in nitrogen atmosphere, where 0.1, 0.5 and 1.0 wt% SWCNT loadings dispersed in the polysulfones increased the initial decomposition temperature (T_i) by about 20, 30 and 45 ºC, respectively, whereas the corresponding increments under dry air were ~18, 25 and 37 ºC. These differences can be explained considering that CNTs are thermally more stable in the former conditions, in agreement with TGA studies performed by other authors [35]. Similar trends were found within the temperatures of maximum rate of weight loss (T_{mr}). In the case of oxidant environment, the stabilization effect was systematically more pronounced for the second stage ($T_{mr\ II}$), probably due to the lower degradation rate of this step.

The comparison of these data with TGA results from similar non-compatibilized samples (Table 2) reveals that the incorporation of PSF or PEES increases considerably the degradation temperatures of PEEK/SWCNT systems. Thus, for compatibilized composites including 1.0 wt% CNT loadings, T_i increases by an average of 20 ºC in comparison to samples reinforced with non-wrapped fillers. Such magnitude of thermal enhancement has only been reported in the literature for a few compatibilized polymer/CNT systems [36,37]. The compatibilizer improves the dispersion of the nanofillers and is expected to enhance their adhesion with the polymer matrix; this should increase the barrier effect of the CNTs, which

effectively hinders the diffusion of the degradation products from the bulk of the polymer to the gas phase, hence slowing down the decomposition process. Moreover, polysulfones possess excellent thermal stability [18], and consequently PEEK/PSF and PEEK/PEES reference blends present slightly higher decomposition temperatures than the pure matrix.

Regarding the influence of the compatibilizer, no significant differences were found between composites incorporating PEES and PSF, as it can be concluded from Table 2, which collects the characteristic temperatures for PEEK/SWCNT composites, the pure compounds and the reference mixtures. Nevertheless, the type of SWCNT seems to affect the decomposition process. Samples including arc-purified SWCNTs exhibit the highest degradation temperatures. This is consistent with the results obtained from TGA study of the SWCNTs (Table 1), which shows that these CNTs are more resistant to oxidation, probably due to their lower metal content, since the residual impurities are known to catalyze the decomposition process [38]. The excellent characteristics of these fillers, combined with their effective dispersion in the polysulfones, which additionally possess superior thermal stability, are synergic effects that lead to a noticeable enhancement in the degradation temperatures of the matrix.

3.4. Crystallization and melting experiments

One of the major issues in thermal analysis is the study of the crystallization and melting behavior of the polymer matrix in the composites, especially the role of the reinforcement entities and compatibilizers in these processes, which strongly influence the macroscopic properties of the materials. To evaluate these effects, PEEK/SWCNT composites incorporating varying concentration of CNTs were subjected to DSC analysis under non-isothermal conditions. Fig. 7a shows, as an example, the crystallization exotherms for PEEK/LG+PSF composites with different CNT content. Interestingly, it can be observed that the addition of 0.1 wt% SWCNT loading dispersed in PSF leads to a slight increase in the crystallization peak

temperature (T_c) of PEEK, whereas at higher concentrations T_c shifts progressively to lower temperatures, the decrease being around 10 ºC for the composite containing 1.0 wt% SWCNTs. Similar trends are found within their apparent crystallization enthalpies ΔH_c, hence the level of crystallinity X_c of the composites. The incorporation of small amounts of wrapped SWCNTs increases the crystallinity of the matrix by an average of 6%, whilst composites including higher concentrations exhibit similar or slightly lower level of crystallinity than pure PEEK. Analogous behavior was observed from the crystallization thermograms of samples including SWCNTs dispersed in PEES. These facts give hint that the addition of CNTs wrapped by polysulfones likely results in two contrary effects on the crystallization behavior of PEEK. Firstly, CNTs supply nucleating sites, consequently increasing T_c. Secondly, they may impede the diffusion and arrangement of the long polymer chains and thereby postpone the overall crystallization process. When a minor CNT content is incorporated in the PEEK matrix, the nucleating effect probably prevails, whereas at higher loadings, although the nucleation surface becomes larger, the formation of a strong CNT network should hinder the crystal growth, leading to lower T_c and X_c for these composites.

To corroborate the above indicated phenomena, two kinetic parameters, the nucleation activity and the effective energy barrier, were determined from DSC curves obtained at different cooling rates. Dobreva and Gutzow [39,40] suggested a simple method for calculating the nucleation activity (NA) of foreign substrates. It is known that this parameter decreases with the addition of nanofillers; it approaches to 0 for extremely active particles, whilst tends to 1 in the case of inert substrates. For homogeneous nucleation, the cooling rate ϕ can be written as $ln\phi = A-(B/\Delta T_p^2)$, while for the heterogeneous case it follows the expression $ln\phi = A-(B^*/\Delta T_p^2)$, where A is a constant, B and B^* are thermodynamic parameters [45] and ΔT_p is the difference between the melting temperature and T_c. Therefore, from the slopes of the linear plots $ln\phi$ *vs.* $1/\Delta T_p^2$ (Fig. 8), the values of B and B^* can be calculated for

PEEK and the composites, respectively, hence the nucleation activity NA = B/B^*. The addition of small amounts of SWCNTs dispersed in PSF causes a reduction in NA, which reaches a value of 0.84 for 0.1 wt% loading; similar results were obtained for the other systems tested, suggesting that low contents of wrapped SWCNTs act effectively as nucleating agents in the PEEK matrix. However, further increase in the filler loading leads to a negative effect on the nucleation process (NA~1), hence makes the crystallization process slower. This dependence of the nucleating activity of the wrapped SWCNTs on the polymer matrix justifies the variations observed in the crystallization temperature and crystallinity of PEEK with the nanofiller content (Fig. 7a).

On the other hand, the crystallization activation energy, or effective energy barrier ΔE, can be used to estimate the growth ability of the chain segments. The higher ΔE, the more difficult is the transport of macromolecular segments to the growing surface. Considering the variation of T_c with ϕ, ΔE could be determined following the Kissinger expression [41]: $\ln (\phi / T_c^2) = A - (\Delta E/R\ T_c)$, where R is the universal gas constant, the rest of the parameters being described previously. ΔE data, obtained from the plots of $ln\ (\phi/T_c^2)$ *vs.* $1/T_c$, are about -447, -440, -434 and -363 kJ/mol for the neat PEEK and its composites with 0.1, 0.5 and 1.0 wt% laser SWCNTs dispersed in polysulfone, respectively. Similar values were found for wrapped arc-purified nanotubes. It is clear that samples with filler concentrations equal or higher than 0.5 wt% display larger ΔE than the pure matrix. This implies that the transport of the macromolecular segments to the growing surface of PEEK should be hindered in these composites with high wrapped nanofiller contents.

To obtain further information about the role of the polysulfones, PEEK/PSF and PEEK/PEES reference mixtures as well as non-compatibilized samples were also analyzed by DSC (Table 3). A small T_c decrease (~5 ºC) was observed for PEEK composites incorporating 1.0 wt% non-wrapped SWCNTs. The comparison with the results obtained for similar

compatibilized composites suggests that the restrictions on polymer chain diffusion and crystal growth become stronger in the presence of the compatibilizing agent. Jin and co-workers, dealing with polypropylene/MWCNT composites [36], also found a decrease in T_c by the incorporation of a compatibilizer, and this effect was attributed to the interactions between the latter and the nanoscale filler occurring during the crystallization process. With regard to the reference blends, their T_c was ~4 ºC lower than that of PEEK, and their ΔH_c slightly decreased, which is comprehensible considering that both PSF and PEES are amorphous polymers miscible with the matrix at very low polysulfone content, which perturb the crystallization process of PEEK. This is a typical behavior of miscible and compatible blends including one non-crystallizing polymer [42,43], attributed to the reduction in chain mobility imposed by the strong interactions between the components. Furthermore, our results are consistent with previous DSC studies of PEEK/PES blends, where a linear decrease in the T_c and crystallinity of PEEK was found upon increasing PES weight fraction [21]. Therefore, the inactive nucleating role of the wrapped nanofillers, the confinement of the matrix chains within the CNT network and the presence of an amorphous compatibilizer might have caused the remarkable decrease in the T_c and the slight reduction in the crystallinity of composites including 1.0 wt% SWCNTs.

The addition of SWCNTs also results in small variations of the melting temperature (T_m) of the PEEK matrix (Fig. 7b), showing similar trends to those observed from the cooling thermograms. In the case of composites including 0.1 wt% SWCNTs dispersed in PSF, T_m increases ~2 ºC, whereas for those incorporating 1.0 wt% CNT content, it decreases around 4 ºC. Moreover, the apparent melting enthalpy ΔH_m and the degree of crystallinity derived from the heating curves X_m also display analogous behavior, showing an increase at low filler contents and a slight decrease at 1.0 wt% CNT loading. However, for similar non-compatibilized composites, T_m and X_m remain merely unaffected by the presence of the

SWCNTs. The aforementioned observations are in contrast to the study reported by Mukherjee *et al*. [37] on polycarbonate/LPC/MWCNT composites, where T_m and the level of crystallinity increased in presence of compatibilizers. This contradiction can be explained considering the poor miscibility between their blend components, where both CNTs and compatibilizers act as heterogeneous nucleating agents. It is also important to notice that a small change in the specific heat associated to the glass transition of the matrix in the composites can be visualized in the heating thermograms. The incorporation of SWCNTs dispersed in the compatibilizer shift this transition towards higher temperatures; this phenomenon will be discussed in detail according to DMA measurements.

A close analysis of Table 3 reveals the influence of the type of nanotube on the crystallization and melting behavior of the matrix; composites incorporating wrapped arc-purified SWCNTs present the highest T_m, T_c and crystallinites. This is consistent with the observations made from the X-ray diffractograms of the nanotubes, which indicated that acid-treated SWCNTs dispersed in the polysulfones are the most effectively disentangled and debundled. Moreover, according to SEM analysis, these SWCNTs present the smallest bundle diameter, hence improved dispersion inside the PEEK matrix; this makes the aforementioned confinement effect less significant, and therefore crystallization occurs at higher temperatures.

3.5. X-ray diffraction analysis

To obtain additional information about the crystalline characteristics of the PEEK matrix in the composite (i.e. structure, crystallization rate, overall crystallinity, crystallite size, etc.), the melting and crystallization processes were monitored by simultaneous SAXS and WAXS experiments, using synchrotron radiation. Fig. 9 shows, as an example, the WAXS patterns of PEEK/laser-grown SWCNTs wrapped in PSF, at 0.1 (a) and 1.0 (b) wt% CNT content, recorded during cooling from the melt to room temperature. In both composites, the main Bragg reflections are observed at 2θ angles of 18.7º, 20.6º, 22.9º and 28.8º, associated to the

diffraction of the (110), (111), (200) and (211) crystalline planes, respectively, of the matrix orthorhombic unit cell [11]. According to the diffractograms, the appearance of crystalline peaks in the compatibilized composite incorporating 0.1 wt% CNT content occurs at around 315 ºC, when the sample reaches a minimum degree of crystallinity. An increase in the intensity of the peaks is found up to 285 ºC (see colored diffractograms on the image), temperature range associated with the growth of polymer crystals, which correlates well with the position of the crystallization peak in the DSC cooling thermogram. On the other hand, the crystalline reflections in the sample including 1.0 wt% wrapped nanotubes appear at ~305 ºC, and become more intense up to 275 ºC; analogous behavior was found for composites including purified arc-grown SWCNTs and PEES as compatibilizer. In the case of non-compatibilized samples, the crystallization initiates at about 310 and 300 ºC, for 0.1 and 1.0 wt% CNT loadings, respectively. These experiments confirm once again that the rate of crystallization of the matrix is influenced by the CNT content, and especially by the presence of the polysulfones. A remarkable change from promotion to retardation is detected as the concentration of wrapped CNTs increases. In contrast, no shift in the position of the Bragg reflections is observed, pointing out that all these composites present the same crystalline structure than pure PEEK.

The degrees of crystallinity X_c were estimated from the approximate relative areas under the amorphous and crystalline peaks of the diffractograms at 25 ºC, and are listed in Table 4 for comparison with DSC results. As it can be observed, both data series agree fairly well and reveal a similar dependence of the crystallinity on the CNT content. The crystallite size (D_{110}) of the composites was calculated from the room temperature diffraction patterns following the Scherrer equation [44], and the values obtained are also included in Table 4. Samples incorporating very small amounts of wrapped CNTs exhibit larger crystals than pure PEEK, whereas those with higher loadings present similar or slightly lower crystal sizes. This

behavior is also consistent with the results obtained from DSC analysis. At very low concentrations, the SWCNT surface favors the nucleation of the matrix crystals, which grow significantly during the cooling stage, leading to higher D_{110} values at 25ºC than PEEK. However, as the concentration increases, the dense CNT network reduces the crystallization rate and confines the crystal growth, resulting in smaller and less perfect crystals. The largest D_{110} are found for samples incorporating wrapped arc-purified SWCNTs, where the increment in comparison to PEEK was ~13%. This is in agreement with the highest T_c and X_c observed in this type of composites. On the other hand, non-compatibilized samples including 1.0 wt% laser-grown nanotubes exhibit the smallest D_{110}, being the decrease nearly 10% in relation to that of the pure matrix.

Fig. 10 shows the development of the long period L as a function of temperature for pure PEEK and composites including different laser-grown SWCNT contents wrapped in PSF. The peak maximum of SAXS diffractograms recorded during heating from room temperature to the melt was used to calculate L ($L=1/s_{max}$) [45], which represents the sum of the average thickness of the crystal lamellae and the interlamellar amorphous regions. All the samples tested exhibit a remarkable increase in the long spacing from ~270 ºC up to the approach of the melting point, temperature range which approximately corresponds to the growth of polymer crystals observed from the WAXS diffractograms (Fig. 9). This evolution of L suggests the existence of rearrangement processes and improvement (i.e. perfection and thickening) of the matrix crystals during the heating cycles subsequent to the crystallization process [11,46]. Furthermore, these recrystallization phenomena could explain the higher crystallinities obtained from DSC heating thermograms in comparison to the values derived from the cooling scans (Table 3).

With regard to room temperature L data for the different concentrations, it can be observed that composites including 0.1 wt% wrapped SWCNTs exhibit larger values than

PEEK, whilst those containing higher concentrations display smaller L. This suggests that the melting behavior of the composites is controlled by the previous crystallization process; the aforementioned change from promotion to reduction in the crystallization rate of PEEK as the CNT content increases is reflected in the formation of larger and smaller crystals than the pure matrix, respectively. Small differences are found among L of composites compatibilized with PSF or PEES (Table 4), since they crystallize approximately at the same temperature and exhibit similar crystallization process, as revealed by WAXS patters. Nevertheless, the non-compatibilized samples present smaller L; thus, at 1.0 wt% CNT loading, it decreases by ~10% in comparison to that of PEEK. On the other hand, differences between L values of the composites and the matrix decrease with increasing temperature, and become negligible (<3%) in the vicinity of the melting point (Fig. 10). This behavior indicates that the effect of reorganization and perfection of the PEEK crystals is favored in the samples with smaller crystal size, and is consistent with the fact that all composites present relatively similar T_m value to that of PEEK, as revealed by DSC heating curves (Fig. 7b).

4. Conclusions

The structure, morphology and thermal properties of high performance semicrystalline PEEK/SWCNT composites incorporating two different polysulfones as compatibilizing agents have been characterized. X-ray diffraction patterns of the SWCNTs dispersed in the polysulfones revealed an effective debundling and disentanglement of the CNTs. Scanning electron microscopy observations showed that the wrapped SWCNTs were homogenously dispersed in the thermoplastic matrix using mechanochemical pre-treatments in an organic solvent followed by a conventional melt-extrusion process. TGA thermograms demonstrated a remarkable increase in the degradation temperatures of the composites by the incorporation of the polysulfones, attributed to the compatibilizing effect and the high thermal stability of these amorphous polymers. The largest thermal enhancement was found for samples including arc-

purified SWCNTs, ascribed to the lower metal content, higher degree of debundling and decomposition temperatures of these CNTs. The addition of 0.1 wt% wrapped SWCNTs increased the crystallization temperature of PEEK, whereas it decreased slightly at higher concentrations, due to the inactive nucleating effect of the nanofillers, the restrictions on chain diffusion imposed by the CNT network and the presence of an amorphous compatibilizer miscible with the matrix. Similar trends were found within the level of crystallinity of the composites, calculated from both DSC and X-ray diffraction measurements. Samples containing very small amount of wrapped SWCNTs exhibited larger crystallite size and long period values than the pure matrix. At higher loadings, the dense CNT network reduced the crystallization rate of PEEK, leading to the formation of smaller and less perfect crystals. Overall, the thermal properties of these composites improved considerably in the presence of the polysulfones, and are well above the required for application in the transport industries.

Acknowledgments

Financial support from a coordinated project between the National Research Council of Canada (NRC) and the Spanish National Research Council (CSIC) is gratefully acknowledged. Dr. A. Diez would like to thank to the Spanish Ministry of Science and Innovation (MICINN) for Juan de la Cierva postdoctoral contract. X-ray diffraction experiments were performed at the Soft condensed Matter A2 beamline of the HASYLAB synchrotron (DESY– Hamburg, I-20090038 EC), supported by the European Commission.

References

[1] Thostenson ET, Ren Z, Chou T-W. Advances in the science and technology of carbon nanotubes and their composites: a review. Compos Sci Technol 2001; 61(13):1899-912.

[2] Dai L, Mau AWH. Controlled Synthesis and Modification of Carbon Nanotubes and C_{60}: Carbon Nanostructures for Advanced Polymeric Composite Materials. Adv. Mater 2001; 13(12-13):899-913.

[3] Yu M-F, Lourie O, Dyer MJ, Moloni K, Kelly TF, Ruoff RS. Strength and Breaking Mechanism of Multiwalled Carbon Nanotubes Under Tensile Load. Science 2000; 287(5453)**:**637-40.

[4] Enomoto K, Kitakata S, Yasuhara T, Ohtake N, Kuzumaki T, Mitsuda Y. Measurement of Young's modulus of carbon nanotubes by nanoprobe manipulation in a transmission electron microscope. Appl Phys Lett 2006; 88(15):15315-7.

[5] Pham JQ, Mitchell CA, Bahr JL, Tour JM, Krishanamoorti R, Greeen PF. Glass transition of polymer/single-walled carbon nanotube composite films. J Polym Sci 2003; 41: 3339-45.

[6] Cochet M, Maser WK, Benito AM, Callejas MA, Martínez MT, Benoit JM, et al. Synthesis of a New Polyaniline/Nanotube Composite: "in situ" Polymerization and Charge Transfer Through Site-Selective Interaction. Chem Commun 2001; 1450-1.

[7] Bafna SS, Sun T, Baird DG. The role of partial miscibility on the properties of blends of a polyetherimide and two liquid crystalline polymers. Polymer 1993; 34(4):708-15.

[8] Staniland PA, "Poly(ether ketone)s". In: Allen G, Bevington JC, editors. Comprehensive Polymer Science, vol. 5, New York: Pergamon Press; 1989, p. 484-97.

[9] Dahl KJ, Jansons V, Polymers and Other Advanced Materials: Emerging Technologies and Business Opportunities. In: Prasad PN, editor. New York: Plenum Press; 1995, p. 69-81.

[10] Searle OB, Pfeiffer RH. Victrex® poly(ethersulfone) (PES) and Victrex® poly(ether ether ketone) (PEEK). Polym Eng Sci 1985; 25(8):474-6.

[11] Naffakh M, Gómez MA, Ellis G, Marco C. Thermal properties, structure and morphology of PEEK/thermotropic liquid crystalline polymer blends. Polym Int 2003; 52(12):1876-86.

[12] Hsiung CM, Cakmak M, White JL.Crystallization phenomena in the injection molding of poly ether ether ketone and its influence on mechanical properties. Polym Eng Sci 1990; 30(16)**:**967-80.

[13] Jonas A, Kegras R. Thermal stability and crystallization of poly(aryl ether ether ketone). Polymer 1991; 32(15):2691-706.

[14] Werner P, Verdejo R, Wöllecke R, Altsadt V, Sandler J, Shaffer MSP. Carbon nanofibers allow foaming of semicrystalline poly(ether ether ketone). Adv Matter 2005; 17:2864-9.

[15] Deng F, Ogasawara T, Takada N. Experimental Characterization of Poly (Ether Ether Ketone/Multi-Wall Carbon Nanotube Composites. Key Eng Mater 2007; 334-335:721-4.

[16] Song L, Zhang H, Zhang Z, Xie S. Processing and performance improvements of SWNT paper reinforced PEEK nanocomposites. Composites A 2007; 38(2):388-92.

[17] Díez-Pascual AM, Naffakh M, Gómez MA, Marco C, Ellis G, Gónzalez-Domínguez JM, et al. Development and characterization of PEEK/carbon nanotube composites. Carbon 2009; 47(13):3079-90.

[18] Nandan B, Kandpal LD, Mathur GN. Poly(ether ether ketone)/ poly(aryl ether sulphone) blends: thermal degradation behaviour. Eur Polym J 2003; 39(1):193-8.

[19] Summers GJ, Ndawuni MP, Summers CA. Chemical modification of polysulfone: anionic synthesis of dipyridyl functionalized polysulfone. Polymer 2001; 42(2):397-402.

[20] Balashova IM, Danner RP, Puri PS, Duda JL. Solubility and Diffusivity of Solvents and Nonsolvents in Polysulfone and Polyetherimide. Ind Eng Chem Res 2001; 40:3058-64.

[21] Ni Z. The Preparation, Compatibility and Structure of PEEK-PES blends. Polym Adv Technol 1994; 5:612-4.

[22] Shibata M, Fang Z, Yosomiya R. A study of blends of poly(ether ether ketone) and poly(ether sulphone): Effect of the addition of poly(ether ether ketone) oligomer. Polymers & polymer composites 1996; 4(7):483-8.

[23] Journet C, Maser WK, Bernier P, Loiseau A, Lamy de la Chapelle M, Lefrant S, et al. Large-scale production of single-walled carbon nanotubes by the electric-arc technique. Nature 1997; 388:756-8.

[24] Yu A, Bekyarova E, Itkis ME, Fakhrutdinov D, Webster R, Haddon RH. Application of centrifugation to the large-scale purification of electric arc-produced single-walled carbon nanotubes. J Am Chem Soc 2006; 128: 9902-8.

[25] Hu H, Yu A, Kim E, Zhao B, Itkis ME, Bekyarova E, Haddon RC. Influence of the zeta potential on the dispersability and purification of single-walled carbon nanotubes. J Phys Chem B 2005; 109:11520-4.

[26] Kingston CT, Jakubek ZJ, Dénomée S, Simard B. Efficient laser synthesis of single-walled carbon nanotubes through laser heating and condensing of the vaporization plume. Carbon 2004; 42(8-9):1657-64.

[27] Blundell DJ, Osborn BN. The morphology of poly(aryl-ether-ether-ketone). Polymer 1983; 24(8):953-8.

[28] Thess A, Lee R, Nikolaev P, Dai H, Petit P, Robert J, et al. Crystalline ropes of metallic carbon nanotubes. Science 1996; 273:483-7.

[29] Dresselhaus MS, Dresselhaus G, Jorio A, Souza AG, Saito R. Raman spectroscopy on isolated single wall carbon nanotubes. Carbon 2002; 40(12):2043-61.

[30] Rols S, Righi A, Alvarez L, Anglaret E, Almairac R, Journet C, et al. Diameter distribution of single wall carbon nanotubes in nanobundles. Eur Phys J B 2000; 18(2): 201-6.

[31] Valentini L, Biagiotti J, Kenny JM, Santucci S. Morphological characterization of single-walled carbon nanotubes-PP composites. Compos Sci Technol 2003; 63(8):1149-53.

[32] Arepalli S, Nikolaev P, Gorelik O, Hadjiev VG, Holmes W, Files B, et al. Protocol for the characterization of single-wall carbon nanotube material quality. Carbon 2004; 42(8-9):1783-91.

[33] Smith Jr MR, Hedges SW, LaCount R, Kern D, Shah N, Huffman GP, et al. Selective oxidation of single-walled carbon nanotubes using carbon dioxide. Carbon 2003; 41(6):1221–30.

[34] Naffakh M, Ellis G, Gomez MA, Marco C. Thermal decomposition of technological polymer blends 1. Poly(aryl ether ether ketone) with a thermotropic liquid crystalline polymer. Polym Degrad Stab 1999; 66(3):405-13.

[35] Walker Jr PL. Carbon: an old but new material revisited. Carbon 1990; 28(2-3):261-79.

[36] Jin HS, Kang CH, Yoon KH, Bang DS, Park Y-B. Effect of Compatibilizer on Morphology, Thermal and Rheological Properties of Polypropylene/functionalized Multi-Walled Carbon Nanotubes Composites. J Appl Polym Sci 2009; 111(2):1028-33.

[37] Mukherjee M, Bose S, Nayak GC, Das CK. A study on the properties of PC/LCP/MWCNT with and without compatibilizers. J Polym Res 2009 (In press).

[38] Pang LSK, Saxby JD, Chatfield SP. Thermogravimetric Analysis of Carbon Nanotubes and Nanoparticles. J Phys Chem 1993; 97(27):6941-2.

[39] Dobreva A, Gutzow I. Activity of substrates in the catalyzed nucleation of glass-forming melts: I. Theory. J Non-Cryst Solids 1993; 162(1-2):1-12.

[40] Dobreva A, Gutzow I. Activity of substrates in the catalyzed nucleation of glass-forming melts. II. Experimental evidence. J Non-Cryst Solids 1993; 162 (1-2):13-25.

[41] Kissinger HE. Variation of peak temperature with heating rate in differential thermal analysis. J Res Natl Bur Stand 1956; 57:217-21.

[42] Bicakci S, Cakmak M. Development of structural hierarchy during uniaxial drawing of PEEK/PEI blends from amorphous precursors. Polymer 2002; 43(1):149-57.

[43] Datta J, Nandi AK. Cocrystallization of poly(vinylidene fluoride) and vinylidene fluoride-tetrafluoroethylene copolymers: 2. Thermodynamic study. Polymer 1996; 37(23):5179-87.

[44] Patterson AL. The Scherrer Formula for X-Ray Particle Size Determination. Phys Rev 1939; 56: 978-82.

[45] Cser F. About the Lorentz correction used in the interpretation of small angle X-ray scattering data of semicrystalline polymers**.** J Appl Poly Sci 2000; 80(12):2300-8.

[46] Krüger KN, Zachmann HG. Investigation of the melting behavior of poly(aryl ether ketones) by simultaneous measurements of SAXS and WAXS employing synchrotron radiation. Macromolecules 1993; 26(19):5202-8.

Figure captions:

Fig. 1 - Chemical structures of poly(ether ether ketone), PEEK (a), poly(bisphenol-A-ether sulfone), PSF (b), and poly(1-4-phenylene ether-ether sulfone), PEES (c).

Fig. 2 - TEM micrographs of arc-purified (a) and laser-grown (b) SWCNTs wrapped in PEES.

Fig. 3 - X-ray diffractograms of laser-grown (a) and arc-purified (b) SWCNTs dispersed in PSF and PEES. As reference, the diffraction patterns of the corresponding non-wrapped nanotubes are also plotted. The comparison between the diffractograms of the laser-grown wrapped SWCNTs and the pure polysulfones is shown in (c).

Fig. 4 - FT-Raman spectra of (a) purified arc-grown SWCNTs and their corresponding dispersions in the polysulfones, (b) pristine and wrapped laser-grown SWCNTs, (c) RBM part of the laser-grown SWCNTs spectra.

Fig. 5 - Typical SEM micrographs at different magnifications from fractured surfaces of compatibilized PEEK/SWCNT (1.0 wt%) composites: (a) and (b) PEEK/LG + PEES; (c) and (d) PEEK/LG + PSF. The arrows show nanotubes randomly dispersed throughout the PEEK matrix.

Fig. 6 - TGA curves for PEEK composites incorporating different amounts of SWCNTs dispersed in PSF, at a heating rate of 10 ºC/min. (a) Inert atmosphere; (b) Oxidative atmosphere. For comparison, only the temperature range between 500 and 650 ºC is plotted.

Fig. 7 - Specific heat flow as a function of temperature recorded during non-isothermal DSC runs of PEEK composites incorporating different SWCNT contents dispersed in PSF, at a rate of 10 ºC/min. (a) Crystallization thermograms. (b) Heating thermograms.

Fig. 8 - Dobreva plots for evaluating the nucleation activity of wrapped laser-grown SWCNTs in PEEK/LG+PSF composites.

Fig. 9 - WAXS diffraction patterns of PEEK/laser-grown SWCNTs dispersed in PSF, at 0.1 (a) and 1.0 (b) wt% CNT content, recorded during cooling from the melt to room temperature, at a

rate of 10 ºC/min. Colored diffractograms correspond to the temperature range associated with the growth of polymer crystals.

Fig. 10 - Long period (L) data as a function of temperature for pure PEEK and composites including different laser-grown SWCNT contents wrapped in PSF. L values were obtained from SAXS diffractograms during heating at 10 ºC/min from room temperature to the melt.

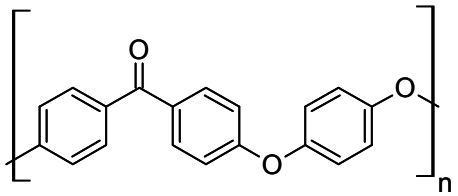

(a)

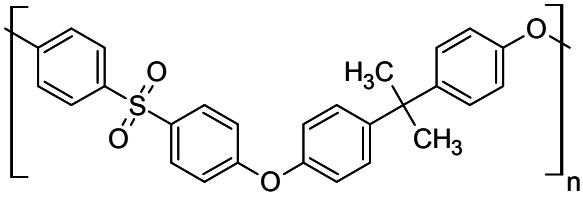

(b)

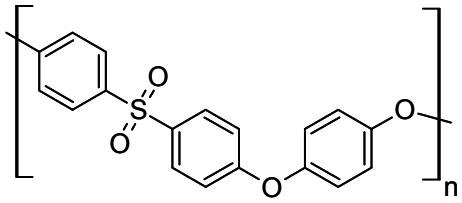

(c)

Fig. 1 - Chemical structures of poly(ether ether ketone), PEEK (a), poly(bisphenol-A-ether sulfone), PSF (b), and poly(1-4-phenylene ether-ether sulfone), PEES (c).

Fig. 2 - TEM micrographs of arc-purified (a) and laser-grown (b) SWCNTs wrapped in PEES.

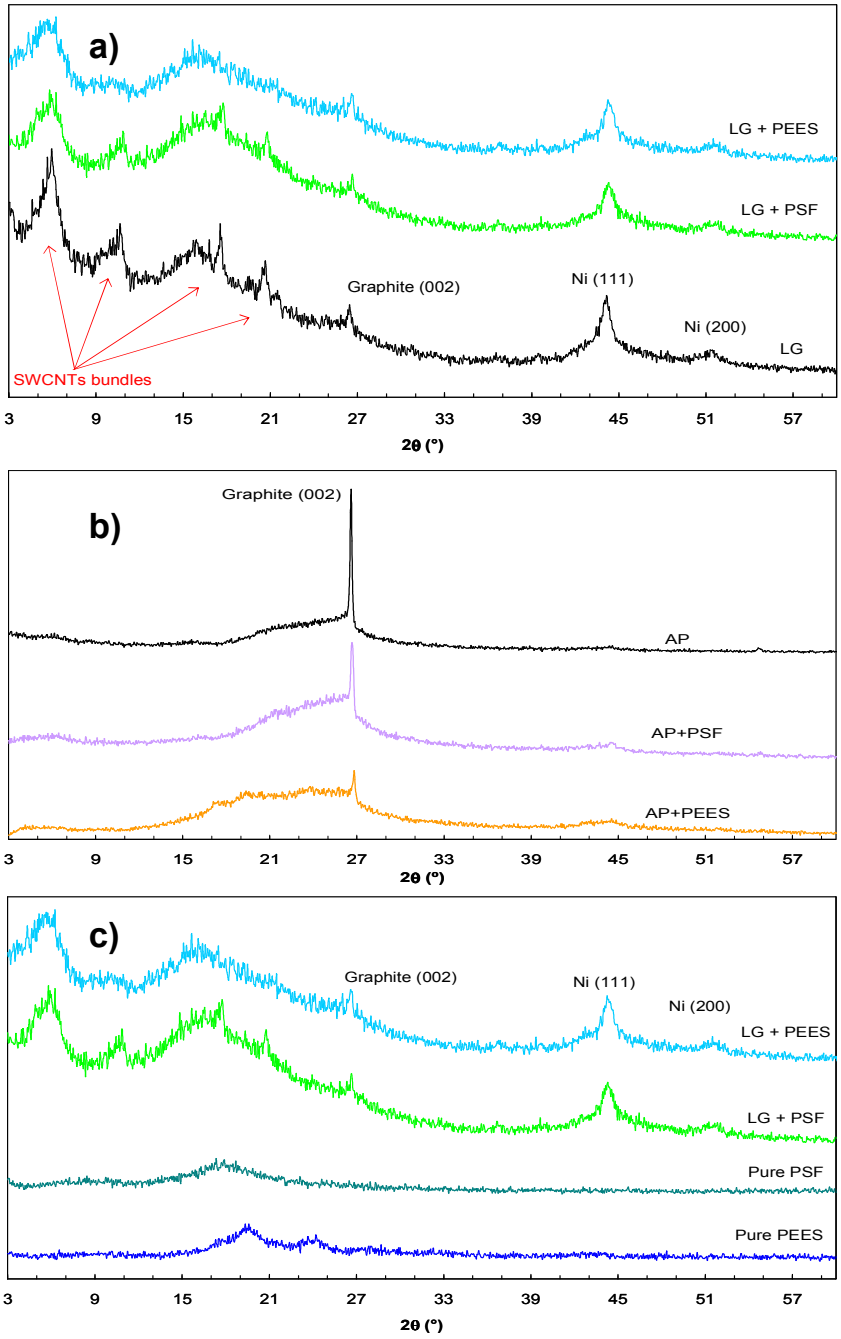

Fig. 3 - X-ray diffractograms of laser-grown (a) and arc-purified (b) SWCNTs dispersed in PSF and PEES. As reference, the diffraction patterns of the corresponding non-wrapped nanotubes are also plotted. The comparison between the diffractograms of the laser-grown wrapped SWCNTs and the pure polysulfones is shown in (c).

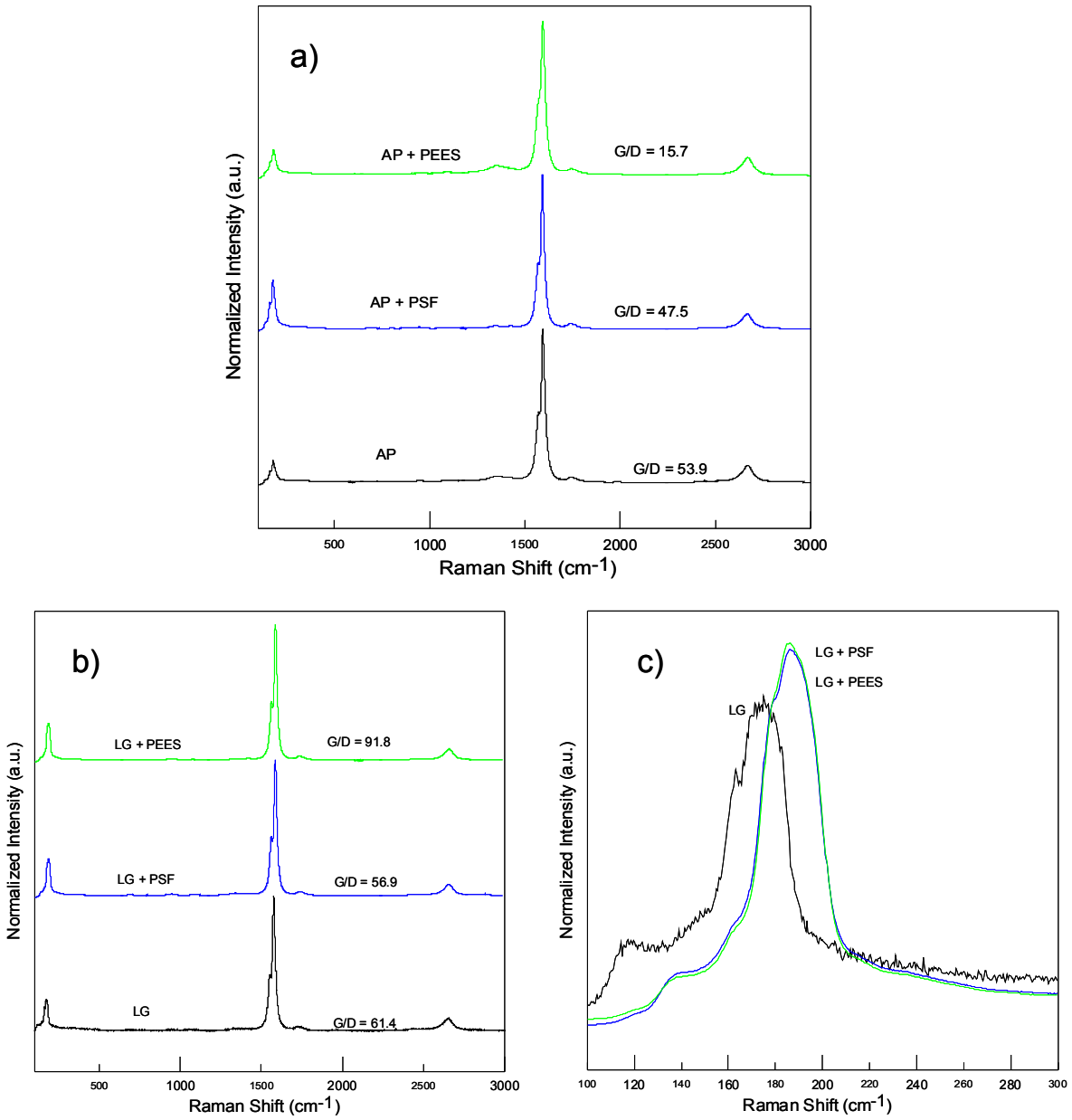

Fig. 4 - FT-Raman spectra of (a) purified arc-grown SWCNTs and their corresponding dispersions in the polysulfones, (b) pristine and wrapped laser-grown SWCNTs, (c) RBM part of the laser-grown SWCNTs spectra.

Fig. 5 - Typical SEM micrographs at different magnifications from fractured surfaces of compatibilized PEEK/SWCNT (1.0 wt%) composites: (a) and (b) PEEK/LG + PEES; (c) and (d) PEEK/LG + PSF. The arrows show nanotubes randomly dispersed throughout the PEEK matrix.

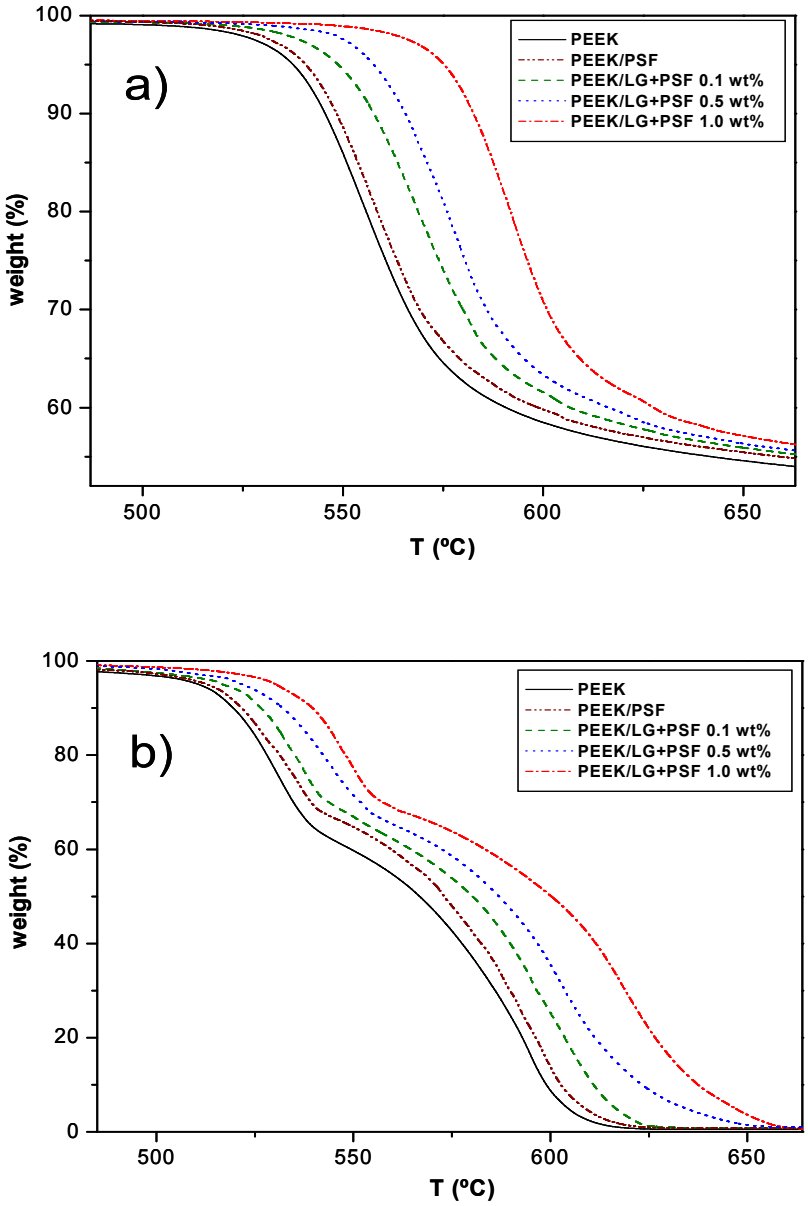

Fig. 6 - TGA curves for PEEK composites incorporating different amounts of SWCNTs dispersed in PSF, at a heating rate of 10 ºC/min. (a) Inert atmosphere; (b) Oxidative atmosphere. For comparison, only the temperature range between 500 and 650 ºC is plotted.

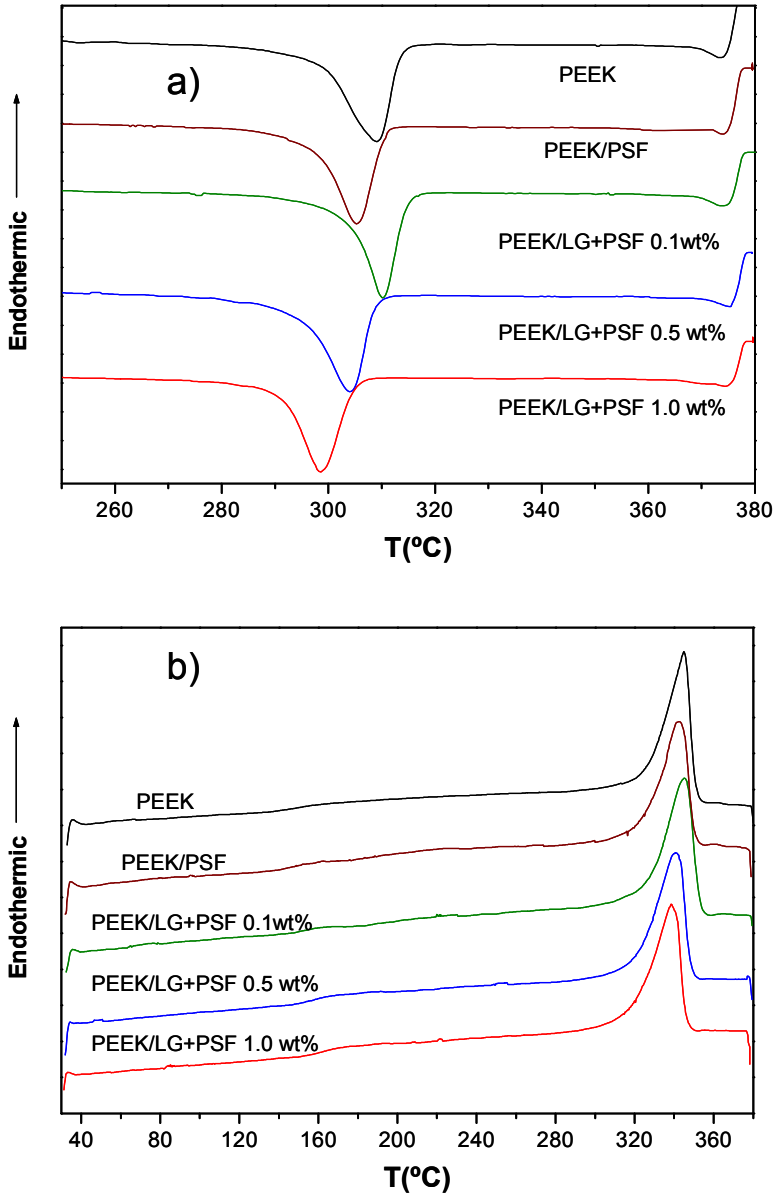

Fig. 7 - Specific heat flow as a function of temperature recorded during non-isothermal DSC runs of PEEK composites incorporating different SWCNT contents dispersed in PSF, at a rate of 10 ºC/min. (a) Crystallization thermograms. (b) Heating thermograms.

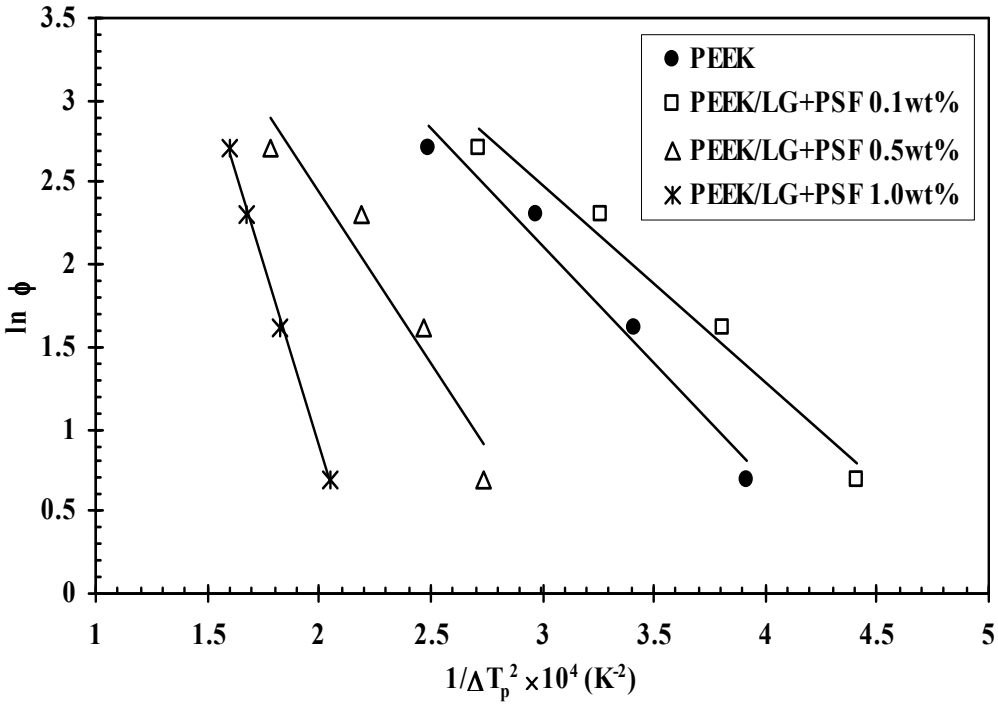

Fig. 8 - Dobreva plots for evaluating the nucleation activity of wrapped laser-grown SWCNTs in PEEK/LG+PSF composites.

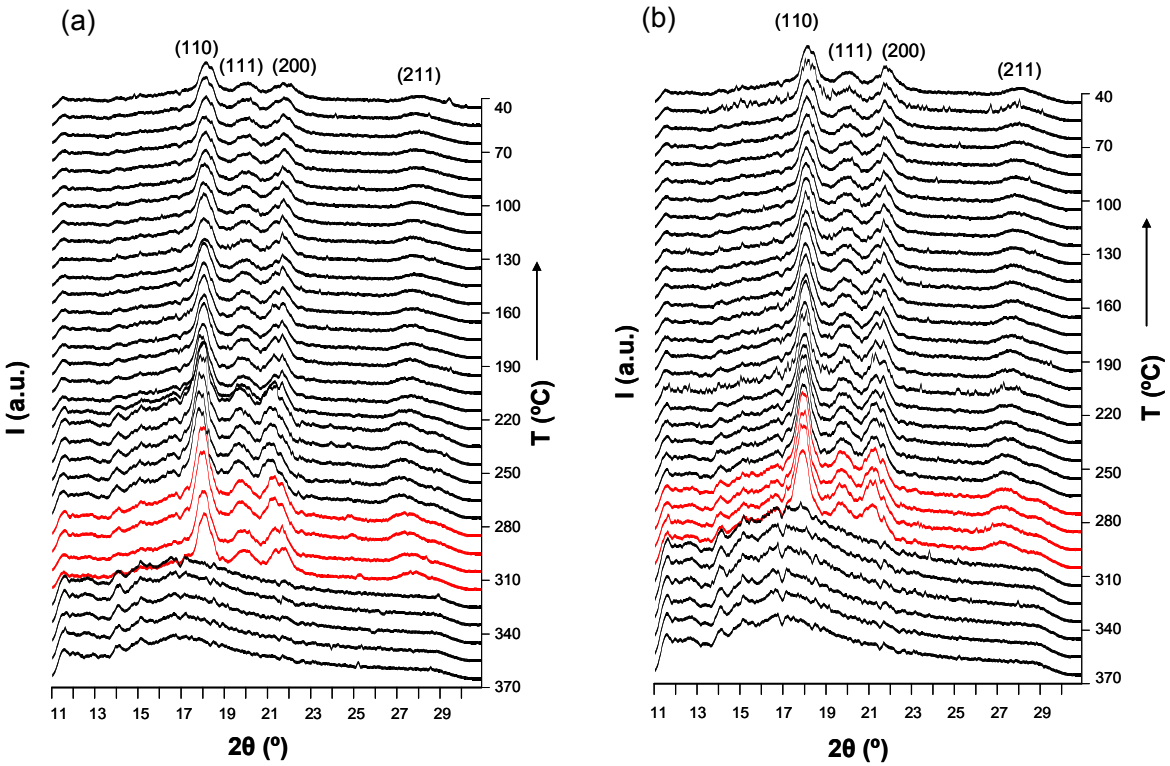

Fig. 9 - WAXS diffraction patterns of PEEK/laser-grown SWCNTs dispersed in PSF, at 0.1 (a) and 1.0 (b) wt% CNT content, recorded during cooling from the melt to room temperature, at a rate of 10 ºC/min. Colored diffractograms correspond to the temperature range associated with the growth of polymer crystals.

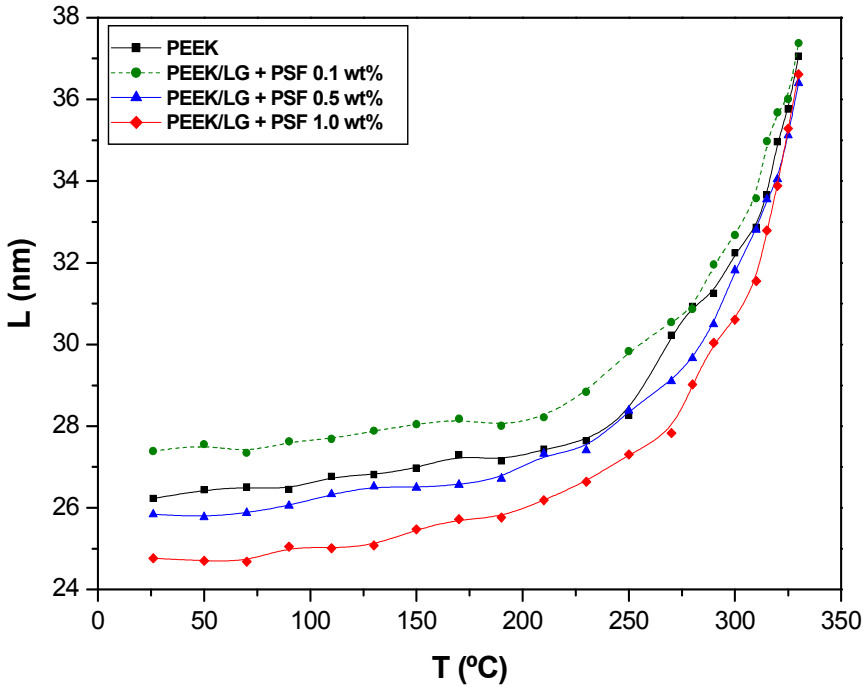

Fig. 10 - Long period (L) data as a function of temperature for pure PEEK and composites including different laser-grown SWCNT contents wrapped in PSF. L values were obtained from SAXS diffractograms during heating at 10 ºC/min from room temperature to the melt.

Tables

Table 1 - Nomenclature and characteristics of the different SWCNTs wrapped in polysulfones employed for the preparation of the PEEK composites.

Sample Code	Preparation Method	Compatibi. (wt%)	Metal (wt%)	T_{mr} (ºC)	D (nm)
AP + PEES	Arc (HNO_3 treated)	PEES (11.2)	1.7	560	17.8
AP + PSF	Arc (HNO_3 treated)	PSF (9.6)	1.8	556	21.4
LG + PEES	Laser (as-grown)	PEES (8.5)	4.1	493	25.5
LG + PSF	Laser (as-grown)	PSF (7.1)	4.3	490	30.1

The compatibilizing agent, metal content and temperature of maximum degradation rate (T_{mr}) were determined from TGA thermograms under air atmosphere. The average bundle diameter D was calculated from SEM micrographs.

Table 2 - Characteristic degradation temperatures of the PEEK/SWCNT composites obtained from TGA measurements under inert and oxidative atmospheres at a heating rate of 10 ºC/min. For comparison, data of the pure compounds and the reference samples are also included in the table.

	Inert atmosphere			Oxidative atmosphere			
	T_i (ºC)	T_{10} (ºC)	T_{mr} (ºC)	T_i (ºC)	T_{10} (ºC)	$T_{mr\,I}$ (ºC)	$T_{mr\,II}$ (ºC)
PEEK	520	544	558	478	520	530	584
PEEK/LG (0.1)	532	547	555	483	523	534	596
PEEK/LG (0.5)	537	553	563	486	528	538	600
PEEK/LG (1.0)	541	558	567	491	531	541	603
PEEK/AP (0.5)	540	555	574	488	527	542	602
PEEK/AP (1.0)	546	566	581	493	532	545	606
PEES	517	548	572	489	522	540	616
PEEK/PEES	520	545	560	480	521	530	585
PEEK/LG+PEES (0.1)	539	559	572	495	525	536	595
PEEK/LG+PEES (0.5)	550	566	580	504	531	545	605
PEEK/LG+PEES (1.0)	563	582	591	511	539	549	620
PEEK/AP+PEES (0.1)	542	557	574	497	527	538	596
PEEK/AP+PEES (0.5)	551	563	582	506	534	546	605
PEEK/AP+PEES (1.0)	566	584	593	517	541	551	622
PSF	536	558	583	494	531	556	621
PEEK/PSF	525	546	561	482	521	532	587
PEEK/LG+PSF (0.1)	537	558	569	494	525	535	594
PEEK/LG+PSF (0.5)	548	562	577	503	532	542	602
PEEK/LG+PSF (1.0)	562	579	589	513	539	547	617
PEEK/AP+PSF (0.1)	538	560	570	496	526	536	595
PEEK/AP+PSF (0.5)	549	565	578	505	534	544	603
PEEK/AP+PSF (1.0)	565	583	590	514	540	548	618

The displayed temperatures are: T_i: initial degradation temperature obtained at 2% weight loss; T_{10}: temperature for 10% weight loss; T_{mr}: temperature of maximum rate of weight loss.

Table 3 - DSC thermal parameters of compatibilized PEEK/SWCNT composites. T_c and T_m designate the crystallization and melting temperatures, respectively. X_c and X_m correspond to the crystallization and melting crystallinities derived from the peak areas. For comparison, data of non-compatibilized samples and the reference mixtures are also included in the table.

Mat. (% SWCNTs)	T_c (ºC)	X_c (%)	T_m (ºC)	X_m (%)	Mat. (% SWCNTs)	Tc (%)	X_c (%)	T_m (ºC)	X_m (%)
PEEK	309.0	42.5	344.2	44.8	PEEK/PSF	305.3	39.8	342.1	42.7
PEEK/LG (0.1)	307.5	44.5	343.5	45.0	PEEK/AP+PEES (0.1)	312.6	46.2	346.1	47.0
PEEK/LG (0.5)	305.1	43.7	343.1	44.3	PEEK/AP+PEES (0.5)	307.4	43.4	344.0	44.9
PEEK/LG (1.0)	303.1	42.3	342.6	43.2	PEEK/AP+PEES (1.0)	303.5	42.1	342.3	44.0
PEEK/AP (0.5)	306.5	44.0	343.1	45.1	PEEK/LG+PSF (0.1)	310.4	44.3	345.3	45.6
PEEK/AP (1.0)	304.0	42.4	342.3	43.6	PEEK/LG+PSF (0.5)	303.9	41.8	341.0	43.8
PEEK/PEES	306.1	40.6	342.4	43.1	PEEK/LG+PSF (1.0)	298.7	40.0	339.8	42.6
PEEK/LG+PEES (0.1)	311.0	45.0	345.7	46.7	PEEK/AP+PSF (0.1)	311.5	46.0	345.9	46.4
PEEK/LG+PEES (0.5)	304.5	42.5	342.8	44.1	PEEK/AP+PSF (0.5)	305.3	43.2	343.5	44.4
PEEK/LG+PEES (1.0)	300.8	41.4	340.7	42.9	PEEK/AP+PSF (1.0)	301.2	41.9	341.9	43.8

Table 4 - Degree of crystallinity X_c, crystallite size D_{110} and long period L values at 25ºC, obtained from WAXS and SAXS diffractograms of the different composites.

Mat. (% SWCNTs)	Xc (%)	D_{110} (nm)	L (nm)	Mat. (% SWCNTs)	Xc (%)	D_{110} (nm)	L (nm)
PEEK	41.4	20.9	26.2	PEEK/PSF	38.9	19.8	23.9
PEEK/LG (0.1)	43.3	20.5	26.1	PEEK/AP+PEES (0.1)	45.1	23.6	28.0
PEEK/LG (0.5)	42.7	19.6	25.2	PEEK/AP+PEES (0.5)	42.2	22.3	26.4
PEEK/LG (1.0)	41.3	18.7	23.9	PEEK/AP+PEES (1.0)	40.9	21.5	25.3
PEEK/AP (0.5)	43.0	20.1	25.5	PEEK/LG+PSF (0.1)	43.3	22.7	27.5
PEEK/AP (1.0)	41.4	19.4	24.0	PEEK/LG+PSF (0.5)	40.6	22.0	25.8
PEEK/PEES	39.1	20.0	23.7	PEEK/LG+PSF (1.0)	39.5	20.1	24.7
PEEK/LG+PEES (0.1)	43.9	23.0	27.4	PEEK/AP+PSF (0.1)	45.0	22.5	27.8
PEEK/LG+PEES (0.5)	41.6	21.9	26.0	PEEK/AP+PSF (0.5)	42.1	21.8	26.1
PEEK/LG+PEES (1.0)	40.4	20.2	24.6	PEEK/AP+PSF (1.0)	40.5	20.7	24.9